Human Molecular Genetics, 2015, Vol. 24, No. 9 2426–2441

doi: 10.1093/hmg/ddv005
Advance Access Publication Date: 9 January 2015
Original Article

ORIGINAL ARTICLE

Nucleolar stress and impaired stress granule formation contribute to *C9orf72* RAN translation-induced cytotoxicity

Zhouteng Tao[1], Hongfeng Wang[1], Qin Xia[1], Ke Li[1], Kai Li[2], Xiaogang Jiang[2], Guoqiang Xu[3], Guanghui Wang[1,5,*] and Zheng Ying[1,4,*]

[1]Laboratory of Molecular Neuropathology, Jiangsu Key Laboratory of Translational Research and Therapy for Neuro-Psycho-Diseases and College of Pharmaceutical Sciences, [2]Department of Pharmacology, College of Pharmaceutical Sciences, [3]Laboratory of Chemical Biology, Jiangsu Key Laboratory of Translational Research and Therapy for Neuro-Psycho-Diseases and College of Pharmaceutical Sciences, [4]Jiangsu Key Laboratory of Preventive and Translational Medicine for Geriatric Diseases, College of Pharmaceutical Sciences, Soochow University, Suzhou, Jiangsu 215021, China and [5]Key Laboratory of Brain Function and Disease, School of Life Sciences, University of Science and Technology of China, Chinese Academy of Sciences, Hefei, Anhui 230027, China

*To whom correspondence should be addressed at: Laboratory of Molecular Neuropathology, Jiangsu Key Laboratory of Translational Research and Therapy for Neuro-Psycho-Diseases and College of Pharmaceutical Sciences, Soochow University, Suzhou, Jiangsu 215021, China. Tel: +86 51265884845; Fax: +86 51265884845; Email: zheng.ying@suda.edu.cn (Z.Y.) or wanggh@suda.edu.cn (G.W.)

Abstract

Amyotrophic lateral sclerosis (ALS) and frontotemporal dementia (FTD) are the two common neurodegenerative diseases that have been associated with the GGGGCC·GGCCCC repeat RNA expansion in a noncoding region of *C9orf72*. It has been previously reported that unconventional repeat-associated non-ATG (RAN) translation of GGGGCC·GGCCCC repeats produces five types of dipeptide-repeat proteins (referred to as RAN proteins): poly-glycine-alanine (GA), poly-glycine-proline (GP), poly-glycine-arginine (GR), poly-proline-arginine (PR) and poly-proline-alanine (PA). Although protein aggregates of RAN proteins have been found in patients, it is unclear whether RAN protein aggregation induces neurotoxicity. In the present study, we aimed to understand the biological properties of all five types of RAN proteins. Surprisingly, our results showed that none of these RAN proteins was aggregate-prone in our cellular model and that the turnover of these RAN proteins was not affected by the ubiquitin–proteasome system or autophagy. Moreover, poly-GR and poly-PR, but not poly-GA, poly-GP or poly-PA, localized to the nucleolus and induced the translocation of the key nucleolar component nucleophosmin, leading to nucleolar stress and cell death. This poly-GR- and poly-PR-mediated defect in nucleolar function was associated with the suppression of ribosomal RNA synthesis and the impairment of stress granule formation. Taken together, the results of the present study suggest a simple model of the molecular mechanisms underlying RAN translation-mediated cytotoxicity in *C9orf72*-linked ALS/FTD in which nucleolar stress, but not protein aggregation, is the primary contributor to *C9orf72*-linked neurodegeneration.

Received: October 1, 2014. **Revised:** December 9, 2014. **Accepted:** January 6, 2015

Introduction

Recent studies showed that an abnormal expansion of a repeated hexanucleotide GGGGCC sequence in a noncoding region of the *C9orf72* gene represents the most common cause of both amyotrophic lateral sclerosis (ALS) and frontotemporal dementia (FTD), two neurodegenerative disorders that present significant clinical and pathological overlap (1–3). Subsequent studies provided further evidence that *C9orf72* hexanucleotide repeat expansion may also play roles in Alzheimer's disease and Huntington's disease (4,5), suggesting both the importance of *C9orf72* and a common molecular pathway in various neurodegenerative disorders. Typically, normal individuals carry 2–23 GGGGCC repeats, whereas *C9orf72*-linked ALS/FTD (referred to as C9ALS/FTD) patients carry an expansion with dozens to thousands of repeats (1,2,6). However, the relationship between the number of repeats and disease onset or progression remains unclear.

Elucidating how the bidirectional transcription of expanded GGGGCC·GGCCCC repeats leads to neurodegeneration and identifying effective therapeutic treatments for C9ALS/FTD have become the two major goals within the field of C9ALS/FTD research. To date, the following three major hypotheses for the mechanisms underlying this disease have been posited. (1) A protein loss-of-function mechanism may be caused by *C9orf72* haploinsufficiency. Although little is known about C9orf72-coding protein function, an interesting recent study showed that the C9orf72 protein may function in endosomal trafficking and autophagy (7). Hexanucleotide repeat expansion might impair the expression of the coding product of *C9orf72*, and it has been widely demonstrated that the *C9orf72* mRNA levels are reduced in patients carrying a *C9orf72* expansion (1–3), suggesting that partial loss of *C9orf72* transcript expression may be associated with disease pathogenesis. In support of this loss-of-function mechanism, studies using animal models, such as the vertebrate zebrafish and the invertebrate *Caenorhabditis elegans*, showed that *C9orf72* depletion caused deficient locomotion and motor neuron degeneration (8,9). However, families carrying a *C9orf72* expansion exhibit a dominant inheritance pattern, which suggests that loss of *C9orf72* function may not be a key mechanism of the disease. (2) An RNA gain-of-function mechanism. To date, most efforts to understand the mechanism underlying C9ALS/FTD have exclusively focused on the contribution of RNA-mediated toxicity toward manifestation of the disease. The formation of RNA foci containing the repeat expansion is a key characteristic of many repeat expansion diseases associated with RNA-mediated toxicity (10). Both sense and antisense RNA foci of *C9orf72* hexanucleotide repeats have been found in C9ALS/FTD patient cells and tissues (11–16), and sequestration and dysregulation of RNA-binding proteins by hairpin and G-quadruplex structures consisting of GGGGCC repeats impair RNA processing and contribute to disease pathogenesis (12,15,17–20). However, it remains unclear whether these RNA-binding proteins associate with endogenous GGGGCC repeats or RNA foci *in vivo*. (3) A protein gain-of-function mechanism. Repeat-associated non-ATG (RAN) translation was initially reported to be associated with spinocerebellar ataxia type 8 (SCA8) and myotonic dystrophy type 1 (DM1), both of which involve a CAG repeat expansion (21). Subsequently, RAN translation products of expanded GGGGCC and CGG repeats were identified in C9ALS/FTD (22,23) and fragile X-associated tremor ataxia syndrome, respectively (24). Shortly thereafter, several studies further demonstrated that the antisense GGCCCC repeat is also RAN translated (13,16,25). Depending on the reading frame of the bidirectional transcript, GGGGCC·GGCCCC repeats encode poly-glycine-alanine (GA), poly-glycine-proline (GP), poly-glycine-arginine (GR), poly-proline-arginine (PR) and poly-proline-alanine (PA) dipeptide repeat-containing proteins, which are referred to as RAN proteins. Although the cytoplasmic and nuclear aggregation of RAN proteins in patient brains suggests that these proteins may be pathogenic (13,16,22,23,25–27), direct evidence for the role of RAN proteins in disease pathogenesis largely remains lacking. Recently and intriguingly, poly-GR and poly-PR were identified to be cytotoxic (28), most likely by interfering with RNA biogenesis in nucleoli (29), suggesting that RAN proteins may play important roles in disease pathogenesis.

Here, we aimed to comprehensively examine the biological properties of these five types of RAN proteins to determine whether and the mechanism by which they contribute to cytotoxicity. Surprisingly and unexpectedly, our results showed that none of the RAN proteins was aggregate-prone and that poly-GR and poly-PR, but not poly-GA, poly-GP or poly-PA, localized to the nucleolus and induced cell death in association with nucleophosmin (B23) translocation from the nucleolus to the nucleoplasm, impaired ribosome RNA biogenesis and stress granule formation. Taken together, the two elegant studies of Kwon *et al.* and Mizielinska *et al.* and our results highlight nucleolar stress as a fundamental biological determinant of neurodegeneration and reveal the molecular mechanism underlying RAN translation-mediated neurotoxicity in ALS/FTD.

Results

Cell death is differentially induced by poly-GR and poly-PR, but not poly-GA, poly-GP or poly-PA, RAN proteins or GGGGCC RNA repeats

To determine whether RAN proteins directly induce cytotoxicity, it was necessary to dissociate the potential toxicity of hexanucleotide RNA repeats from that of RAN protein repeats. Thus, we generated constructs encoding RAN proteins that contained non-GGGGCC repeats, such as GGAGCA repeats that encoded poly-GA and GGAAGA repeats that encoded poly-GR, which were referred to as 'synthetic' constructs. The synthetic constructs were predicted to lack the ability to produce RNA foci and other RAN proteins because they could not form putative hairpin structures, in contrast to GGGGCC·GGCCCC repeats (Supplementary Material, Fig. S1). We also generated ATG start codon-initiated GGGGCC and CCGGGG constructs that encoded all five RAN proteins using various reading frames, which were referred to as 'pathogenic' constructs (Fig. 1A).

All of the above-mentioned GFP-tagged constructs, each of which contained 30 repeat sequences, and a GFP-tagged construct containing a repeated GGGGCC sequence lacking an ATG (No ATG) were transfected into cells. The constructs (both synthetic and pathogenic) that encoded arginine-containing poly-dipeptides (poly-GR or poly-PR) strikingly induced cell death in both neuronal (NSC-34) and non-neuronal (HEK293) cells (Fig. 1B and C). Given that the GGGGCC RNA repeats alone (No ATG) exhibited very weak toxicity following an extended transfection period compared with poly-GR and poly-PR (Fig. 1D and E), we reasoned that the five RAN proteins encoded by the pathogenic constructs containing ATG-preceded GGGGCC and CCGGGG repeats should display toxicity following a standard transfection period. In support of this notion, the GGGGCC- and non-GGGGCC-encoded RAN proteins, such as poly-GA and poly-GR, exerted similar cytotoxic effects (Fig. 1B and C). These observations were further confirmed by the MTT assay (Supplementary Material, Fig. S2).

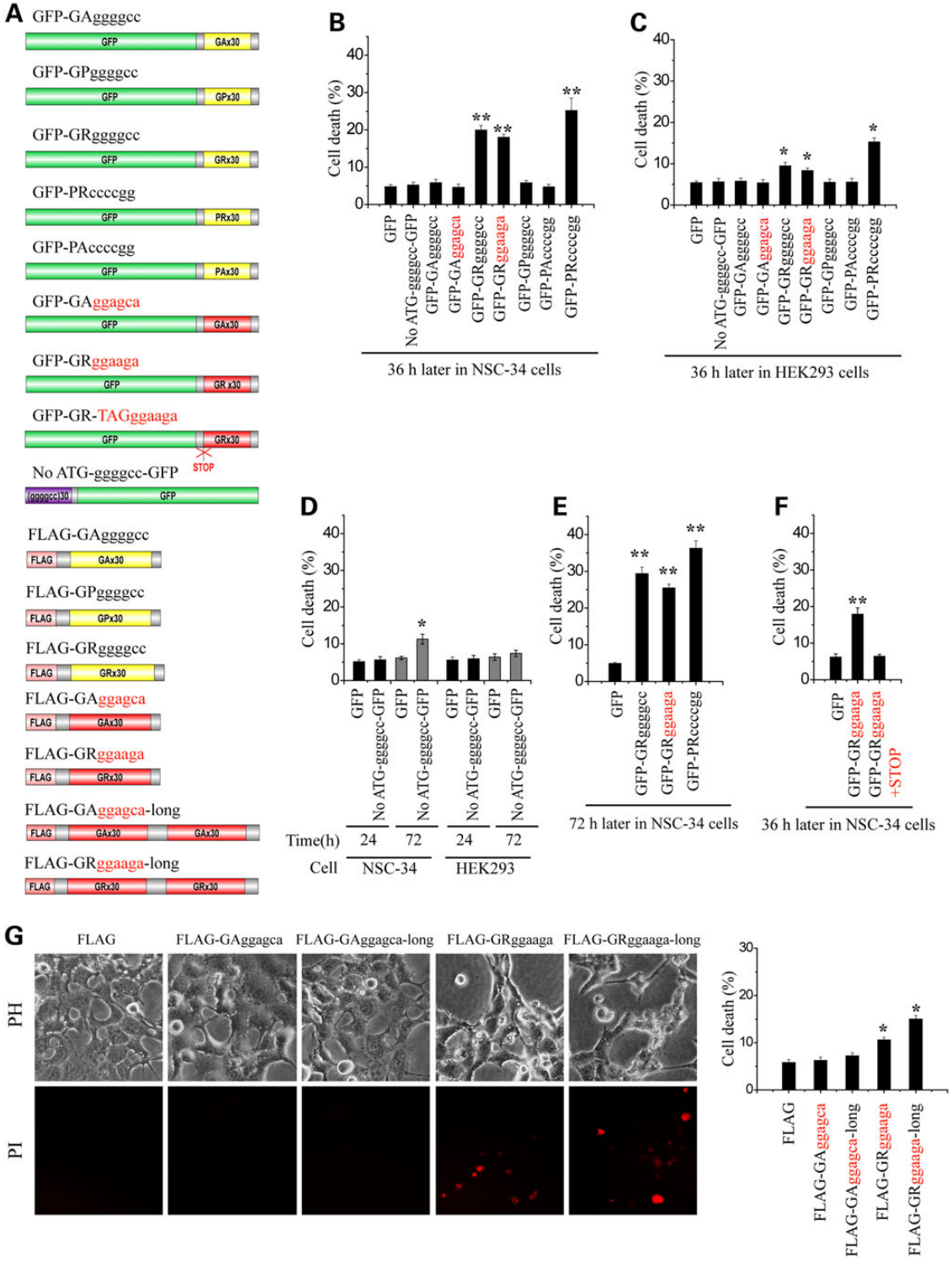

Figure 1. Selective cell death induced by poly-GR and poly-PR, but not poly-GA, poly-GP, poly-PA RAN proteins or GGGGCC RNA repeats alone. (**A**) Schematic diagram of the hexanucleotide repeat constructs used in this study. Essentially, these constructs contained 30 synthetic or pathogenic hexanucleotide repeats. For example, GAggggcc indicates GA(ggggcc)$_{30}$. We termed the constructs with 60 hexanucleotide repeats 'long'. For example, GAggagca-long indicates GA(ggggcc)$_{60}$. (**B** and **C**) NSC-34 or HEK293 cells were transfected with the GFP tag alone or a GFP-tagged RAN construct as indicated. Thirty-six hours later, the cells were subjected to PI staining to count the dead cells. The quantitative data are indicated as the means ± SEM, $^{*}P < 0.05$, $^{**}P < 0.01$. (**D**) NSC-34 or HEK 293 cells were transfected with GFP or a GFP-tagged GGGGCC lacking an ATG (No ATG) for 36 or 72 h. Then, the cells were subjected to PI staining. The quantitative data are indicated as the means ± SEM, $^{*}P < 0.05$. (**E**) NSC-34 cells were transfected with GFP, GFP-GRggggcc, GFP-GRggaaga or GFP-PRccccgg. Cell death was analyzed via PI staining 72 h later. The quantitative data are indicated as the means ± SEM, $^{**}P < 0.01$. (**F**) NSC-34 cells were transfected with GFP, GFP-GRggaaga or GFP-GRggaaga containing a TAG stop codon, and 36 h later, the cells were subjected to PI staining. The quantitative data are indicated as the means ± SEM, $^{**}P < 0.01$. (**G**) HEK293 cells were transfected with FLAG, FLAG-GAggagca, FLAG-GAggagca-long (containing 60 repeats), FLAG-GRggaaga or FLAG-GRggaaga-long (containing 60 repeats). Thirty-six hours later, cell death was measured via PI staining, and the cell morphology was shown using PH microscopy. The quantitative data of cell death are indicated as the means ± SEM, $^{*}P < 0.05$.

To further confirm that cytotoxicity was initiated by the RAN protein repeats but not the RNA repeats, we added a TAG stop codon 5′ to the GGAAGA sequence. This manipulation completely abolished the cytotoxicity induced by synthetic poly-GR (Fig. 1F), indicating that the synthetic poly-GR used in our study perfectly mimicked the toxic properties of the pathogenic poly-GR. To determine whether the cytotoxicity induced by arginine-containing RAN proteins is repeat length-dependent and to exclude the possibility that the artificial tag was responsible for the effect, we transfected cells with FLAG-tagged constructs encoding 60 repeats of synthetic poly-GA or poly-GR (referred to as 'long') and found that the 60-repeat poly-GR displayed higher cytotoxicity than the 30-repeat poly-GR. However, neither the 60-repeat nor the 30-repeat poly-GA had any effect on cytotoxicity (Fig. 1G). Similar observations were obtained using NSC-34 cells (data not shown), suggesting that longer repeat expansions in arginine-containing RAN proteins induce more cytotoxicity.

The arginine-enriched RAN proteins poly-GR and poly-PR form 'aggregate'-like inclusion bodies in the nucleus

To determine the physiological role of these RAN proteins, we transfected HEK293 and neuronal cells with GFP- or FLAG-tagged RAN proteins and examined the cellular localization of those RAN proteins using fluorescence microscopy. The results showed that poly-GA, poly-GP and poly-PA were diffusively expressed throughout the cell (in both the nucleus and cytoplasm), whereas poly-GR and poly-PR, the two arginine-enriched RAN proteins, formed structures resembling protein aggregates in the nucleus, similar to a previous observation from polyglutamine (polyQ) inclusion bodies (Fig. 2A, B and E). Notably, pathogenic and synthetic poly-GA and poly-GR displayed similar subcellular localization (Fig. 2A, D and E), which was not affected by the tag or the repeat length (Supplementary Material, Fig. S3). In addition, we found that poly-GR could also diffusely distribute in the cytoplasm and partially diffuse in the nucleus (Fig. 2A and C), whereas poly-PR displayed an exclusively nuclear distribution (Fig. 2A, C and E).

None of the five RAN proteins or nuclear 'aggregates' formed by poly-GR and poly-PR are highly regulated by the ubiquitin–proteasome system (UPS) or autophagy.

Because all RAN proteins have been found in aggregates in C9ALS/FTD brains and because the most remarkable characteristic of protein aggregates is that they are tightly associated with and regulated by the UPS or autophagy (30–32), we examined whether these 'aggregate'-like inclusion bodies were formed by misfolded poly-dipeptides, similar to polyQ protein aggregates, and whether UPS and autophagy targeted these inclusion bodies for protein degradation. Therefore, we transfected cells with RAN proteins and treated the cells with the proteasomal inhibitor MG132 and the autophagy inhibitor Bafilomycin A1 (Baf A1). Surprisingly, no change in the number of nuclear 'aggregates' or in the protein levels of poly-GR or poly-PR was observed after this treatment (Fig. 3A and B), which was consistent with the finding that the nuclear 'aggregates' formed by poly-GR and poly-PR were not changed in Atg5 knockout (autophagy-deficient) mouse embryonic fibroblasts (MEFs) compared with Atg5 wild-type (autophagy-competent) MEFs (Fig. 3D). Additionally, the other three RAN proteins were not generally degraded via the UPS or autophagy (Fig. 3B) and were not aggregate-prone, as inhibiting the UPS and autophagy failed to induce their aggregation (Fig. 3A). We also found that the 60-repeat RAN proteins were not affected by the inhibition of the UPS and autophagy (data not shown). In contrast, the number of polyQ protein (Htt-60Q) aggregates was strikingly increased in MG132-treated cells (Fig. 3C) and in Atg5 knockout cells (data not shown). Taken together, our results suggest that neither the proteasomal nor the autophagy pathway strongly regulates the formation of nuclear inclusion bodies by the two arginine-containing RAN proteins or any other RAN proteins.

The nuclear inclusion bodies formed by poly-GR and poly-PR localize to the nucleoli but are not protein aggregates

As the nuclear inclusion bodies were not affected by the UPS or autophagy, the characteristics of these nuclear inclusions remained unclear. Next, we examined whether these inclusions are associated with the markers of protein aggregates, such as ubiquitin. We also examined VCP/p97 (VCP) and optineurin (OPTN) because these proteins have been well characterized to be associated with ALS/FTD and to be involved in protein quality control systems, such as the UPS and autophagy. As shown in Supplementary Material, Figure S4, none of these proteins colocalized with the nuclear inclusion bodies composed of poly-GRs (Supplementary Material, Fig. S4A–C). In contrast, the nuclear inclusions composed of full-length and truncated ataxin-3 containing an expanded polyQ sequence clearly colocalized with ubiquitin (Supplementary Material, Fig. S4D). These data suggest that the nuclear inclusion bodies formed by arginine-containing RAN proteins are not actual protein aggregates.

To better understand the properties of these inclusions, we evaluated the morphological characteristics of the nuclear inclusion bodies formed by poly-GR using phase contrast (PH) microscopy. We found that these inclusions localized to the nucleoli, which appeared dark under PH conditions (Fig. 4A). In contrast, nuclear inclusion bodies composed of polyQ-expanded ataxin-3 did not colocalize with the nucleolar marker protein B23 (Fig. 4B). To further confirm the nucleolar localization of the arginine-containing RAN proteins, we employed another nucleolar marker protein, nucleolin (NCL). The colocalization of poly-GRs and the nucleolar markers was clearly observed using confocal microscopy (Fig. 4C and D). In addition, poly-PR localized to the nucleoli (data not shown), indicating that the nuclear inclusion bodies formed by poly-GR and poly-PR include nucleolar arginine-enriched RAN proteins but not protein aggregates.

poly-GR and poly-PR, but not other RAN proteins, specifically induce B23 translocation and nucleolar stress

To elucidate the biological consequences of the selective nucleolar localization of poly-GR and poly-PR, we examined the cells at the time when poly-GR and poly-PR began to kill the cells. Both RAN proteins tended to display an exclusively nuclear distribution from 24 to 48 h post-transfection (Fig. 5A). Moreover, during that period, the poly-GR and poly-PR-transfected cells exhibited nucleolar swelling and increased nucleoplasmic translocation of B23, a nucleolar stress sensor and a marker of nucleolar stress that exhibits protective properties (33,34) (Fig. 5B and C).

To gain further insight into the abnormal nucleolar changes mediated by arginine-enriched RAN proteins, we employed mass spectrometry-based proteomic analysis to identify the binding partners of the arginine-enriched RAN proteins, revealing an interactome that included 40S/60S ribosomal proteins, heterogeneous nuclear ribonucleoproteins (hnRNPs), B23 and 14 other proteins that strongly interacted with synthetic poly-GR (Fig. 5E). Among these proteins, most were nucleolar proteins or RNA-binding proteins associated with RNA granules. Moreover,

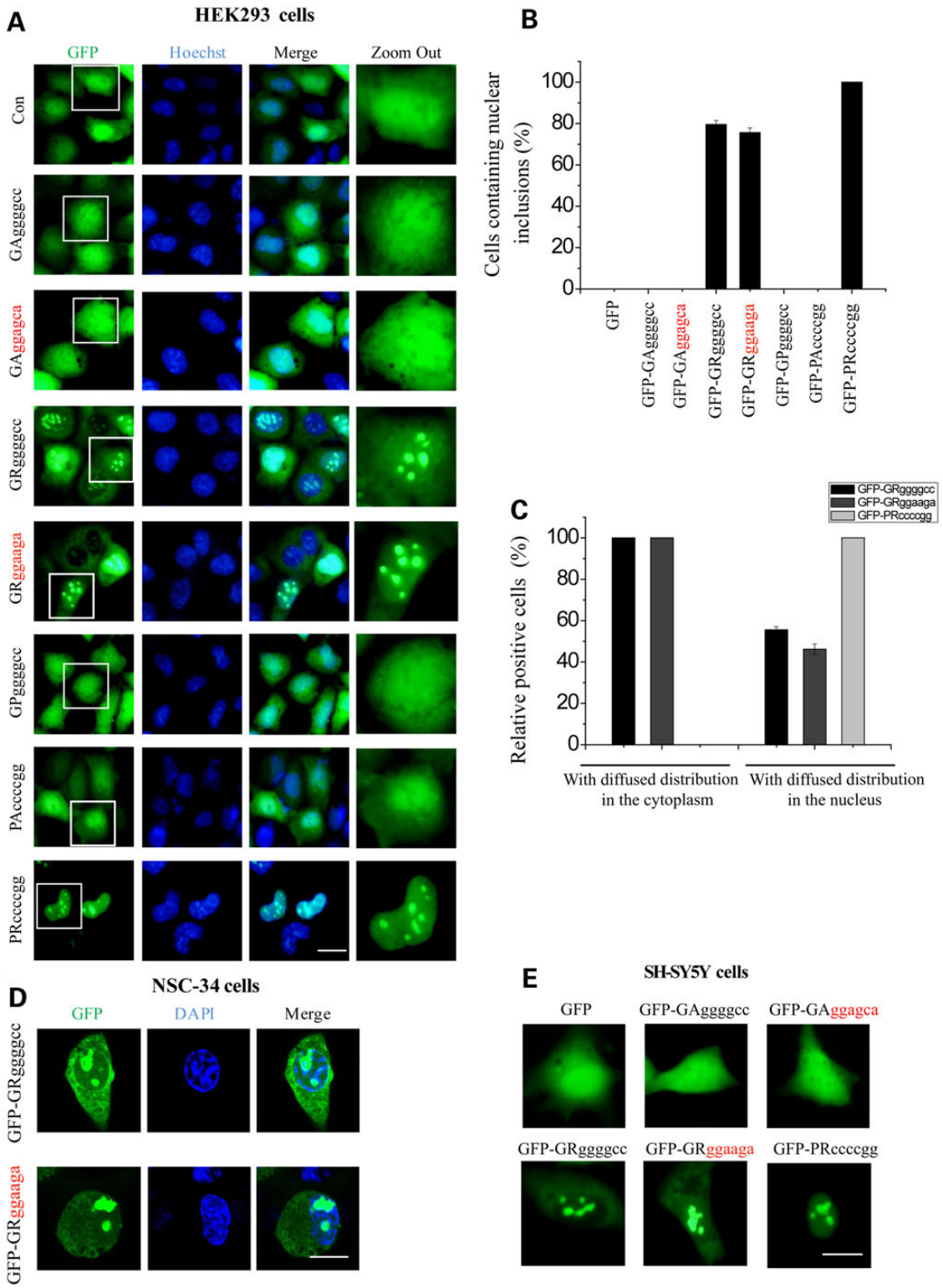

Figure 2. Arginine-enriched RAN proteins form nuclear 'aggregate'-like inclusions. (**A**) HEK293 cells were transfected with GFP, GFP-GAggggcc, GFP-GAggagca, GFP-GRggggcc, GFP-GRggaaga, GFP-GPggggcc, GFP-PAccccgg or GFP-PRccccgg. Twenty-four hours later, the cells were stained with Hoechst (blue) to visualize the nuclei. Subsequently, live cell imaging was performed using fluorescence microscopy. (**B**) The percentages of the cells containing 'aggregates' in A are quantified. (**C**) The transfected cells in A with RAN protein diffusely distribute in the cytoplasm and nucleus were quantified. (**D**) NSC-34 cells were transfected with GFP-tagged GRggggcc or GRggaaga. Then, the cells were fixed 24 h post-transfection and stained with DAPI. (**E**) SH-SY5Y cells were transfected with GFP, GFP-GAggggcc, GFP-GAggagca, GFP-GRggggcc, GFP-GRggaaga or GFP-PRccccgg. Twenty-four hours later, the cells were subjected to microscopic observation. The scale bars represent 10 μm.

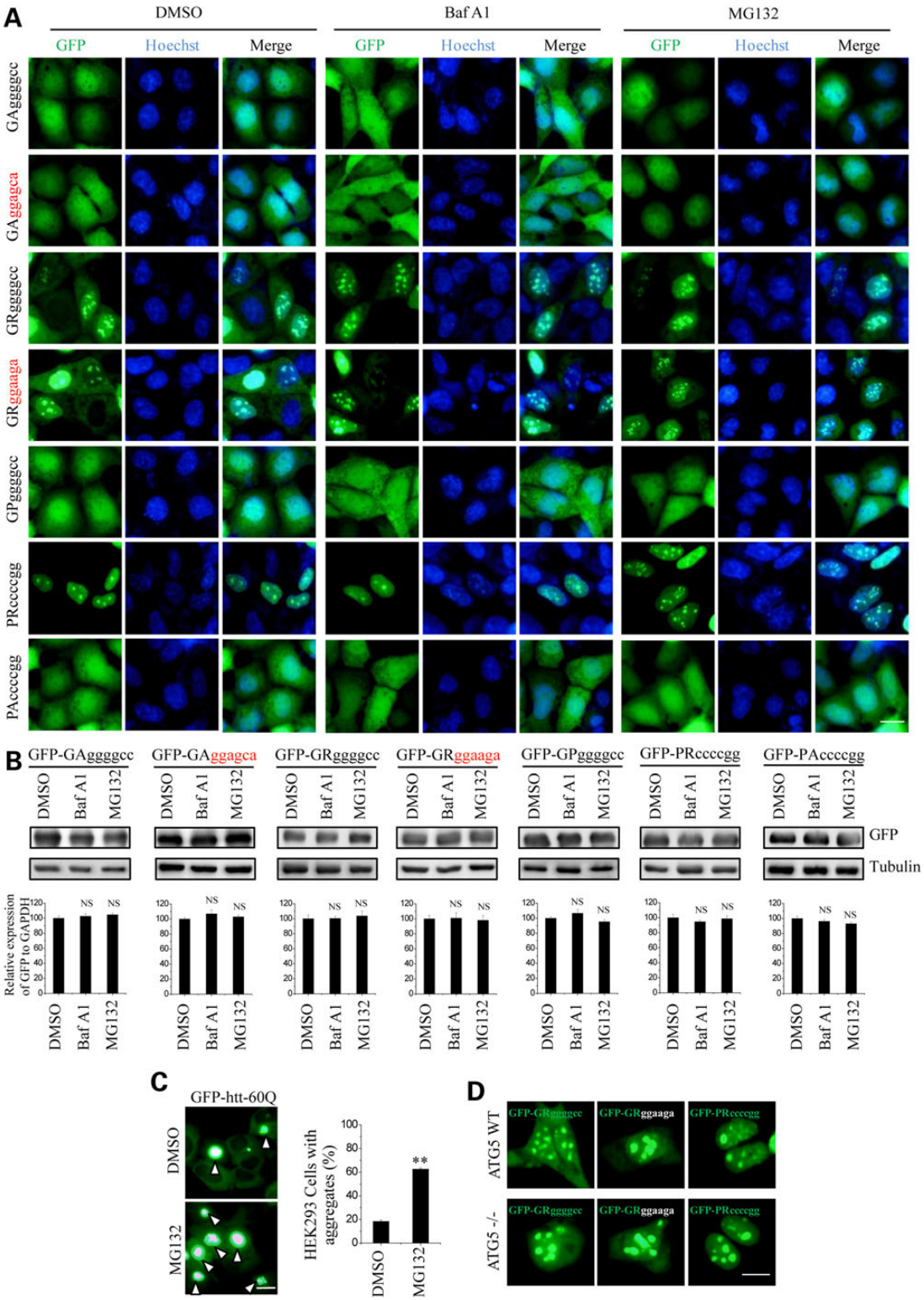

Figure 3. None of the five RAN proteins or the nuclear 'aggregates' formed by poly-GR and poly-PR was associated with UPS or autophagy. (**A**) HEK293 cells were transfected with various GFP-tagged hexanucleotide repeat constructs. Twenty-four hours later, the cells were incubated in 100 nM Baf A1 and 10 μM MG132 for 12 h. Then, the cells were fixed and stained with DAPI. The scale bars represent 10 μm. (**B**) HEK293 cells were transfected and treated with the inhibitors described in A for 12 h. Then, cell lysates were collected and subjected to immunoblot using the indicated antibodies. The protein levels from three independent experiments were quantified (lower panel). The quantitative data are indicated as the means ± SEM, NS, no significance. (**C**) HEK293 cells were transfected with GFP-tagged Htt-60Q. Twenty-four hours later, the cells were treated with DMSO or MG132 for 12 h. Then, the cells were observed using fluorescence microscopy, and the numbers of Htt-60Q aggregates were quantified. The quantitative data are indicated as the means ± SEM; $^{**}P < 0.01$. The scale bars represent 10 μm. (**D**) GFP-GRggggcc, GFP-GRggaaga or GFP-PRccccgg was transfected into ATG5 wild type (ATG5 WT) or ATG5 knockout (ATG5−/−) MEFs. Twenty-four hours later, the cells were visualized using fluorescence microscopy. The scale bars represent 10 μm.

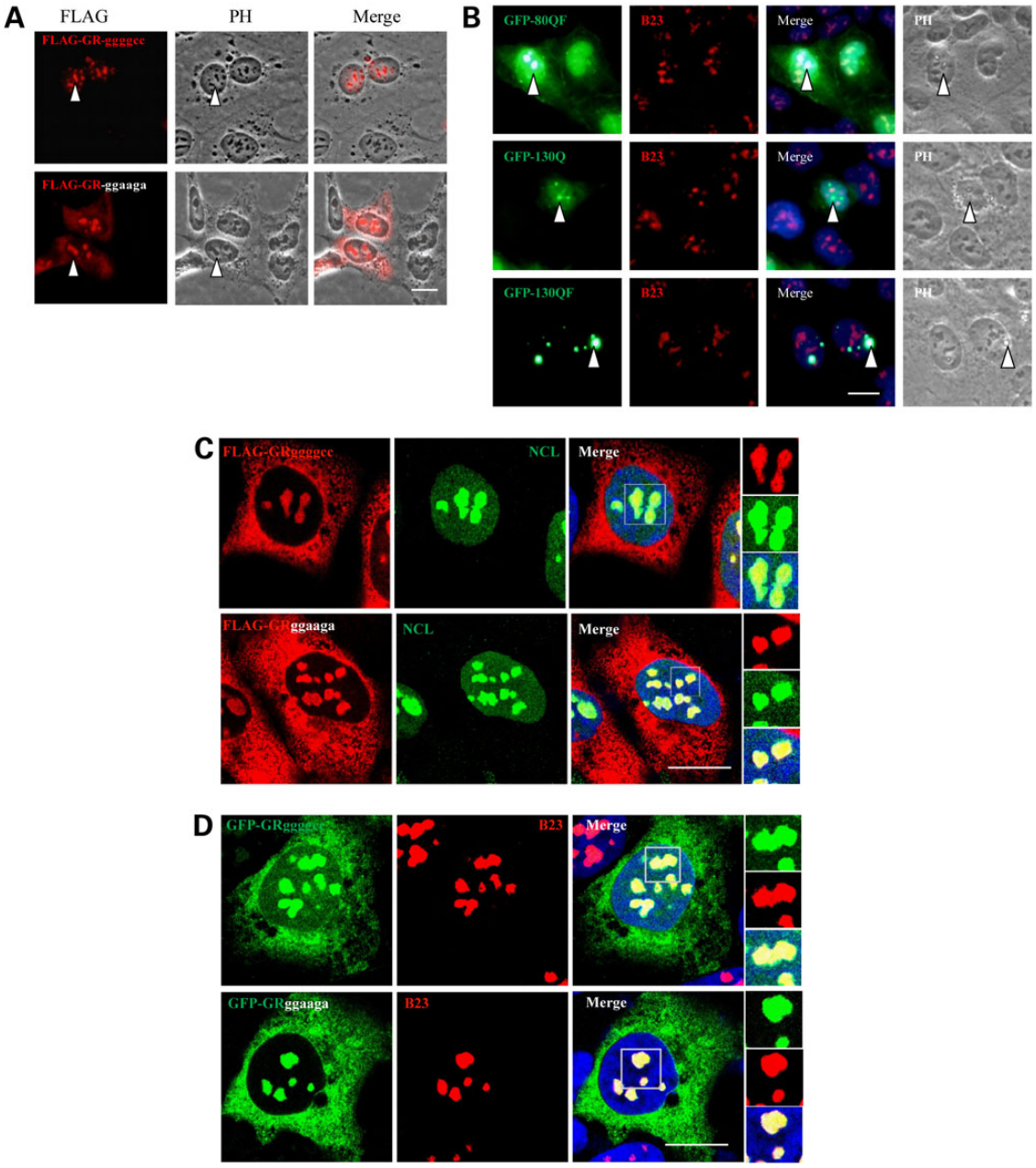

Figure 4. The nuclear inclusions formed by GR and PR are localized to the nucleolus. (**A**) HEK293 cells were transfected with FLAG-tagged GRggggcc or GRggaaga. Twenty-four hours later, the cells were observed under PH microscopy. Arrowheads indicate the nucleoli. (**B**) HEK293 cells were transfected with GFP-tagged full-length or truncated ataxin-3. Twenty-four hours later, the cells were subjected to immunofluorescence staining using an anti-B23 antibody (red) and stained with DAPI. Arrowheads indicate the aggregates formed by polyQ proteins. (**C**) HEK cells were transfected as described in A. Twenty-four hours later, the cells were fixed and stained with anti-FLAG (red) and anti-NCL antibodies (green). (**D**) HEK293 cells were transfected with GFP-GRggggcc or GFP-GRggaaga. Twenty-four hours later, the cells were subjected to immunofluorescence using an anti-B23 antibody (red) and stained with DAPI. The scale bars indicate 10 μm.

B23 co-immunoprecipitated with poly-GR and poly-PR (Fig. 5D, and Supplementary Material, Fig. S5), further confirming that the latter two factors are two nucleolar proteins that are associated with essential components in the nucleolus, such as B23. Taken together, our data suggest that poly-GR and poly-PR may cause morphological changes in the nucleolus and the translocation of B23 from the nucleolus to the nucleoplasm potentially by directly associating with nucleolar components.

The nucleolus is the site where ribosomal RNA is synthesized and the nascent ribosome is assembled, and B23 directly regulates ribosome biogenesis and pre-ribosomal particle transport (33,35). We hypothesized that poly-GR- and poly-PR-mediated B23 translocation might lead to defects in nucleolar function and ribosomal RNA biogenesis. To address this issue, we evaluated the maturation 18S and 28S rRNA, which are processed from the precursor 45S rRNA in RAN protein-expressing cells. The qRT-PCR data showed that both the 18S and 28S rRNA levels were remarkably decreased following the expression of poly-GR or poly-PR (Fig. 6A). In contrast, poly-GA expression increased the 18S and 28S rRNA levels (Fig. 6A). Similar results were obtained using NSC-34 cells (data not shown).

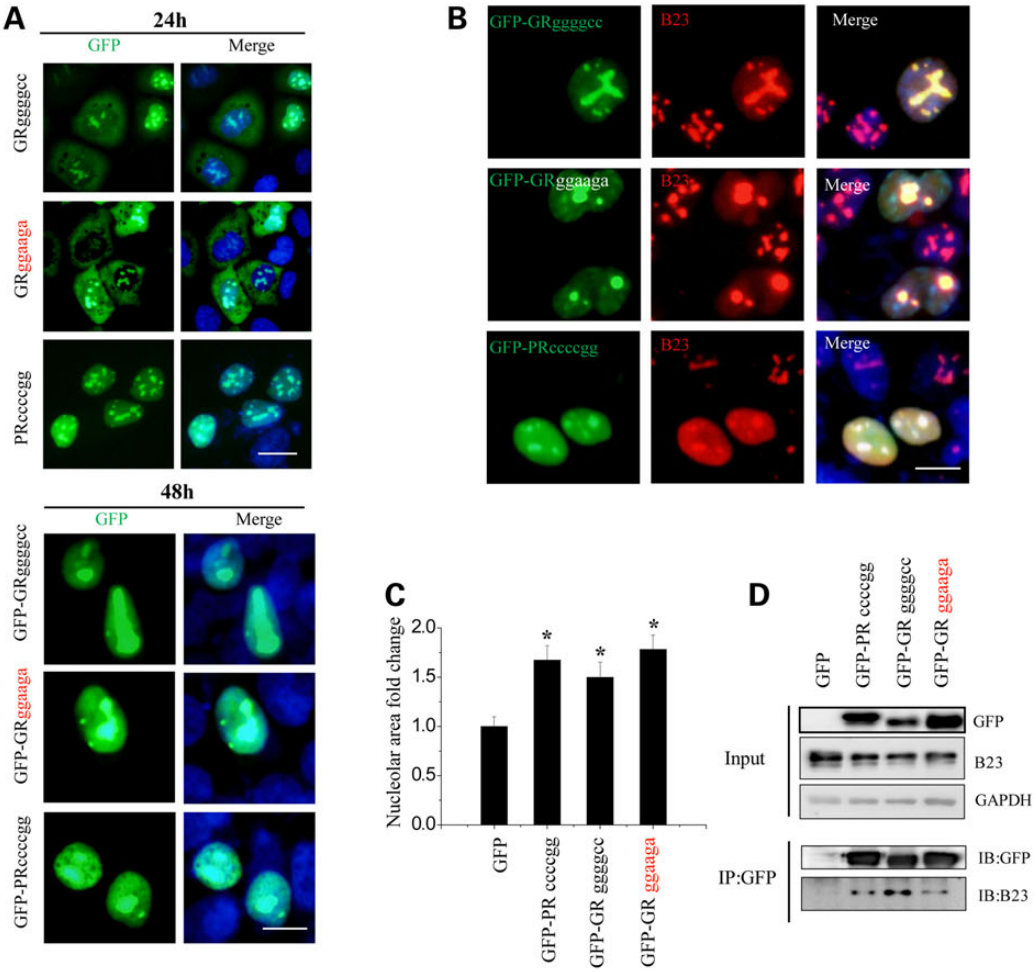

E

Accession	Description	Σ Coverage	Σ# Proteins	Σ# Unique Peptides	Σ# Peptides	Σ# PSMs	MW [kDa]	calc. pI
IPI00643522.1	40S Ribosomal protein S6	20.18	4	3	3	27	25.00	11.14
IPI00003918.6	60S ribosomal protein L4	23.19	8	9	9	17	47.67	11.06
IPI00299573.12	60S ribosomal protein L7a	23.31	7	6	6	19	29.98	10.61
IPI00479630.4	Fragile X mental retardation syndrome-related protein 1 isoform 3	18.1	4	5	5	6	59.88	6.77
IPI00016250.6	Fragile X mental retardation syndrome-related protein 2	14.47	1	6	6	6	77.02	6.60
IPI00013881.6	Heterogeneous nuclear ribonucleoprotein H	10.47	4	2	3	3	49.20	6.30
IPI00514561.1	Heterogeneous nuclear ribonucleoprotein K	19.39	6	5	5	7	47.50	5.63
IPI00414696.1	Heterogeneous nuclear ribonucleoproteins A2/B1 isoform A2	14.96	4	3	3	7	36	8.65
IPI00479630.4	Heterogeneous nuclear ribonucleoprotein U-like protein 1 isoform3	18.1	4	5	5	6	59.9	6.77
IPI00456887.2	Heterogeneous nuclear ribonucleoprotein U-like protein 2	3.61	1	2	2	3	85.1	4.91
IPI00220740.1	Nucleophosmin(B23) isoform 2	25.28	6	4	4	13	29.40	4.61
IPI00301323.1	ATP-dependent RNA helicase DDX18	16.72	3	8	8	10	75.36	9.50
IPI00297900.4	ATP-dependent RNA helicase DDX10	4.11	2	3	3	3	100.80	8.63
IPI00005904.3	ATP-dependent RNA helicase DDX20	1.82	1	1	1	1	92.20	6.95

Figure 5. Poly-GR and poly-PR, but not other RAN proteins, specifically induce B23 translocation from the nucleolus to the nucleoplasm. (**A**) GFP-GRggggcc, GFP-GRggaaga or GFP-PRccccgg was transfected into HEK293 cells. After 24 or 48 h, the cells were stained with Hoechst to visualize the nuclei. The merged images show the colocalization of the GFP and Hoechst fluorescent signals. (**B**) HEK293 cells were transfected with GFP-GRggggcc, GFP-GRggaaga or GFP-PRccccgg. Forty-eight hours later, the cells were fixed and subjected to immunofluorescence using an anti-B23 antibody (red) and stained with DAPI. The scale bars indicate 10 μm. (**C**) HEK293 cells transfected with the indicated plasmid were fixed 48 h after transfection and stained with an anti-B23 antibody and DAPI. The size of the nucleoli, as indicated by B23 staining, from 50 transfected cells was analyzed. The quantitative data are expressed as the means ±SEM, $^*P < 0.05$. (**D**) HEK293 cells were transfected as described in B. Forty-eight hours later, cell lysates were collected and subjected to immunoprecipitation using an anti-GFP antibody. Co-immunoprecipitated B23 was detected using an anti-B23 antibody. (**E**) HEK293 cells were transfected with GFP-GRggaaga. The GFP-immunoprecipitated samples were subjected to mass spectrometric analysis. The list contains 14 proteins that associated with GFP-GRggaaga.

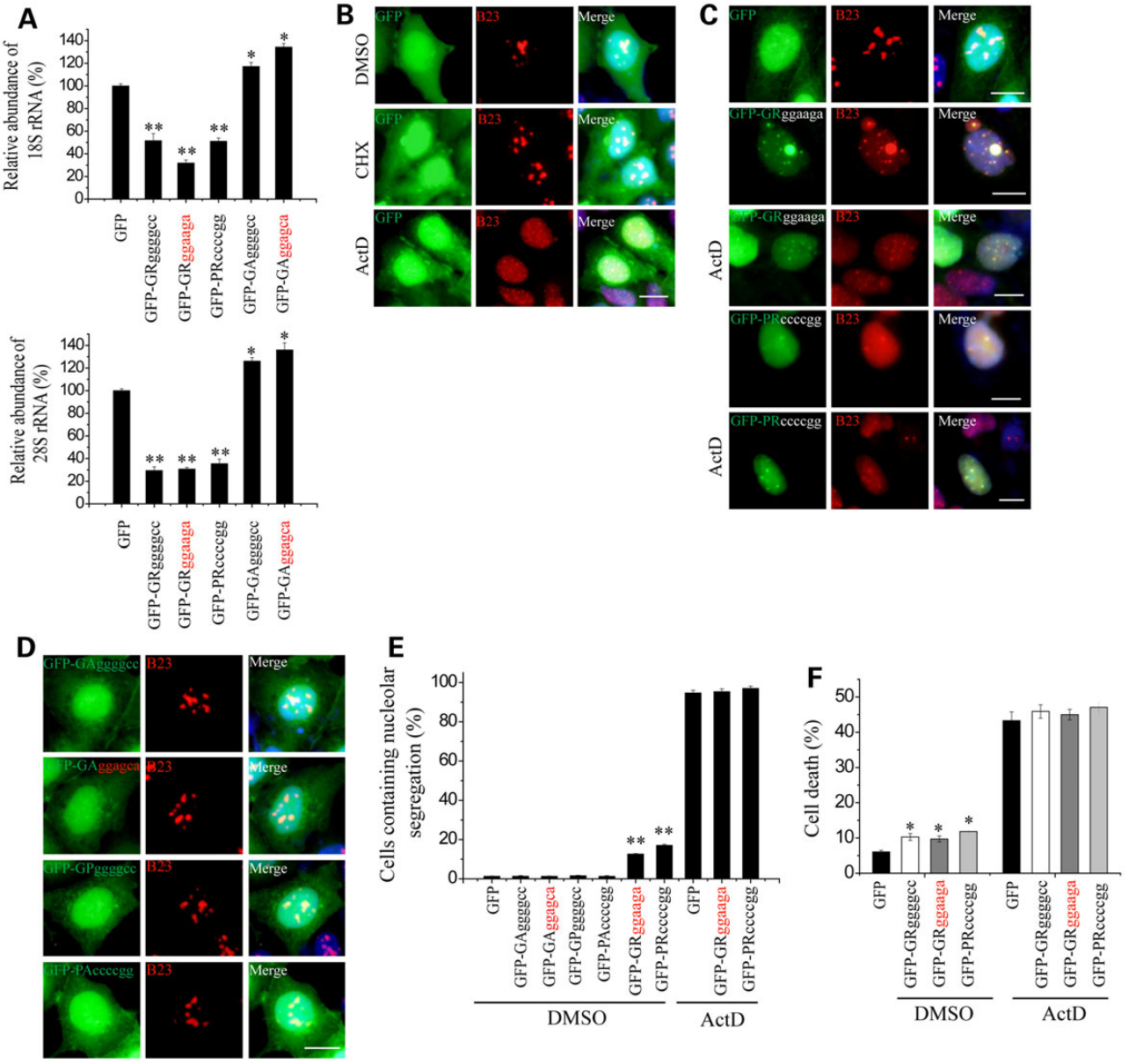

Figure 6. Poly-GR and poly-PR, but not other RAN proteins, specifically impair ribosomal RNA biogenesis and induce nucleolar stress. (**A**) Total RNA was extracted from HEK293 cells 48 h after transfection with GFP, GFP-GRggggcc, GFP-GRggaaga, GFP-PRccccgg, GFP-GAggggcc or GFP-GAggagca. The 18S and 28S rRNA levels were analyzed via qPCR. The quantitative data are expressed as the means ± SEM, $^{*}P < 0.05$; $^{**}P < 0.01$. (**B**) GFP was transfected into HEK293 cells. Forty-eight hours later, the cells were incubated in CHX (100 μg/ml) for 12 h and ActD (0.04 μg/ml) for 4 h. Then, the cells were subjected to immunofluorescence using an anti-B23 antibody (red) and stained with DAPI. (**C**) GFP, GFP-GRggaaga or GFP-PRccccgg was transfected into HEK293 cells. Seventy-two hours later, the cells were incubated in ActD (0.04 μg/ml) for 4 h. Then, the cells were subjected to immunofluorescence using an anti-B23 antibody (red) and stained with DAPI. (**D**) HEK293 cells were transfected with GFP-GAggggcc, GFP-GAggagca, GFP-GPggggcc or GFP-PAccccgg. Seventy-two hours later, the cells were fixed and stained with an anti-B23 antibody (red) and DAPI. The merged images show GFP, B23 and DAPI fluorescent signals. The scale bars indicate 10 μm. (**E**) The quantitative data of nucleolar segregation in B–D are indicated as the means ± SEM, $^{**}P < 0.01$. (**F**) HEK293 cells were transfected with GFP, GFP-GRggggcc, GFP-GRggaaga or GFP-PRccccgg. Twenty-four hours after transfection, the cells were treated with DMSO or ActD (0.04 μg/ml) for 24 h. Then, cell death was measured via PI staining. The quantitative data of cell death are indicated as the means ± SEM, $^{*}P < 0.05$.

To further elucidate the mechanism by which RAN proteins induce cytotoxicity, we treated cells with actinomycin D (ActD), a well-established chemical that induces nucleolar stress (36), to mimic nucleolar stress and compared the characteristics of ActD-treated cells with those of RAN product-transfected cells. ActD treatment strongly induced nucleolar segregation (a morphological change in the nucleolus that reflects a nucleolar functional defect), as shown in Supplementary Material, Figure S6 and Figure 6B that small nucleolar fragments (10–30 small dots double-labeled by B23 and NCL) were scattered across the nucleus after ActD treatment, and B23 translocation to the nucleoplasm (Supplementary Material, Fig. S6, and Fig. 6B) as previously reported (33), whereas the protein synthesis inhibitor cycloheximide (CHX) failed to induce nucleolar segregation or B23 translocation (Fig. 6B). Importantly, our results showed that poly-GR and poly-PR, but not poly-GA, poly-GP or poly-PA, strikingly

induced nucleolar segregation and B23 translocation after an extended transfection period, similar to the results of ActD treatment (Fig. 6C and D). Furthermore, poly-GR and poly-PR expression in combination with ActD exerted the same effect on nucleolar segregation, B23 translocation and cell death as ActD treatment alone (Fig. 6C–F), indicating that the arginine-containing RAN proteins and ActD function in the same pathway that is closely associated with nucleolar stress. Taken together, our results identified nucleolar stress as a potential fundamental contributor to RAN translation-mediated C9ALS/FTD and revealed that this mechanism is specifically triggered by arginine-containing RAN proteins but not other RAN proteins.

Arginine-containing and non-arginine-containing RAN proteins exerted opposite effects on stress granule formation

Next, we examined whether RAN proteins affect stress granules, which are mRNA- and RNA-binding protein-enriched cytoplasmic compartments that associate with multiple proteins involved in ALS/FTD (37,38). We transfected cells with the RAN constructs and analyzed stress granule formation by visualizing the classic stress granule marker protein G3BP1. Surprisingly and interestingly, our results showed that poly-GA, poly-GP and poly-PA induced stress granule formation under normal conditions (Fig. 7A and D), whereas poly-GR and poly-PR, as well as ActD, strikingly inhibited stress granule formation in cells treated with arsenite, a stress granule inducer (Fig. 7B, C, E and F), suggesting that a functional association between RAN proteins and stress granules may contribute to neurodegeneration.

Discussion

Although great efforts and rapid progress have been made to elucidate the mechanism of C9ALS/FTD in the 3 years because a mutation in the *C9orf72* gene was identified as the predominant cause of ALS/FTD (39), whether the repeat expansion in the non-coding region of *C9orf72* initiates neurodegeneration via a loss-of-function or a gain-of-function mechanism remains unclear. Our present findings, along with findings recently reported by McKnight, Isaacs and Partridge groups, reveal a novel mechanism by which this hexanucleotide repeat expansion may cause disease: a gain-of-function mechanism caused by unconventionally translated arginine-containing RAN proteins, which are associated with nucleolar stress and impaired RNA and protein (RNP) homeostasis.

In the case of a loss-of-function mechanism, homozygous patients would be expected to develop a more severe clinical phenotype and a distinct disease spectrum. With this expectation in mind, the finding that a homozygous patient fell within the typical range of disease symptoms (40) suggests that a gain-of-function mechanism likely plays a primary role in C9ALS/FTD. In support of this concept, knockdown of *C9orf72* transcripts, including mRNAs, using antisense oligonucleotides (ASOs) did not exert a toxic effect on iPSC-derived motor neurons (12,41) but rather improved the gene expression profile of these cells (41). Moreover, reducing *C9orf72* expression in the mouse nervous system did not induce neuropathological defects (14), suggesting that a gain-of-function, rather than a loss-of-function, mechanism might be the predominant cause of C9ALS/FTD.

In the case of a gain-of-function mechanism, a fundamental question underlying *C9orf72* hexanucleotide repeat expansion-mediated neurodegeneration is whether it is caused by RNA- or protein-induced toxicity. Although several studies reported that the RNA-mediated toxicity of GGGGCC repeats may be associated with neurodegeneration, given that 'pure' GGGGCC RNA repeats lacking an ATG start codon may continue to produce RAN proteins in cells (16,23), it remains possible that the RAN proteins actually contributed to the neurotoxicity observed in those studies. Here, we successfully distinguished the potential toxicity caused by hexanucleotide RNA repeats from that caused by RAN proteins using synthetic RAN proteins that lacked the potential for RNA toxicity, such as poly-GA, which was encoded by GGAGCA, and poly-GR, which was encoded by GGAAGA. In cells that were transfected in parallel, we found that the GGGGCC repeat alone (No ATG), poly-GA, poly-GP and poly-PA did not display strong toxicity under normal conditions, whereas both pathogenic poly-GR and synthetic poly-GR were strikingly toxic to the cells (Fig. 1). In general, poly-PR displayed greater toxicity than that of poly-GR, possibly due to the stronger nuclear localization of poly-PR (Figs 1 and 2). Although 30-repeat GGGGCC alone displayed very weak cytotoxicity after an extended period (Fig. 1), based on the results reported by Zu *et al*. that a 30-repeat GGGGCC sequence was sufficient to induce RAN translation (16), we propose that the weak damage induced by GGGGCC repeats alone in our study may have resulted from RAN proteins, such as poly-GR, which were produced by GGGGCC repeats. Taken together, our findings indicate that the poly-GR and poly-PR RAN proteins, rather than the hexanucleotide RNA repeats, might represent the primary toxic species responsible for the neurodegeneration observed during C9ALS/FTD. Consistent with our findings, Mizielinska *et al*. reported that poly-GA and poly-PA, as well as GGGGCC 'RNA-only' repeats containing stop codons, did not exhibit any toxicity in *Drosophila* (28). This recent study, together with ours, provides strong evidence that poly-GR and poly-PR products may play a greater role in C9ALS/FTD than do other RAN translation products, including poly-GA, poly-GP and poly-PA.

The next issue was whether RAN protein aggregates contribute to C9ALS/FTD. RAN translation of GGGGCC·GGCCCC repeats leads to the formation of aggregates of RAN polypeptides in patients. Although the contribution of these 'RAN aggregates' to disease pathogenesis remains unclear, they may be closely associated with disease pathogenesis, similar to the role of polyQ proteins in polyQ disorders. Nevertheless, in our cell culture model, we did not detect the formation of classic protein aggregates of RAN proteins that resembled polyQ-containing protein aggregates (Supplementary Material, Fig. S4A–D), even following treatment with a proteasome inhibitor or an autophagy inhibitor that are widely used to induce protein aggregation (Figs 3 and 4). Considering that the RAN proteins in patients may contain thousands of repeats, constructs that induce a higher expression level and longer repeat expansion, rather than the 30–60 repeats used in the current study, need to be employed to evaluate the aggregation and cytotoxicity of RAN proteins in the future. In addition, to further examine the role of RAN protein aggregation in human disease, *in vivo* experiments using rodent models need to be performed to determine whether RAN protein aggregation occurs in the long term and to verify whether it is a pre- or post-symptomatic event. However, notably, no correlation between poly-GA aggregation and the degree of neurodegeneration in C9ALS/FTD patients was detected (42). Furthermore, accumulated poly-GP remained in *C9orf72* ALS iPSC-derived neurons after ASO treatment despite a reduction in neurotoxicity, suggesting that the aggregation of poly-GA and poly-GP may not be a predominant mediator of neurotoxicity in C9ALS/FTD (12). In addition, poly-G, poly-A and poly-P polypeptides were not

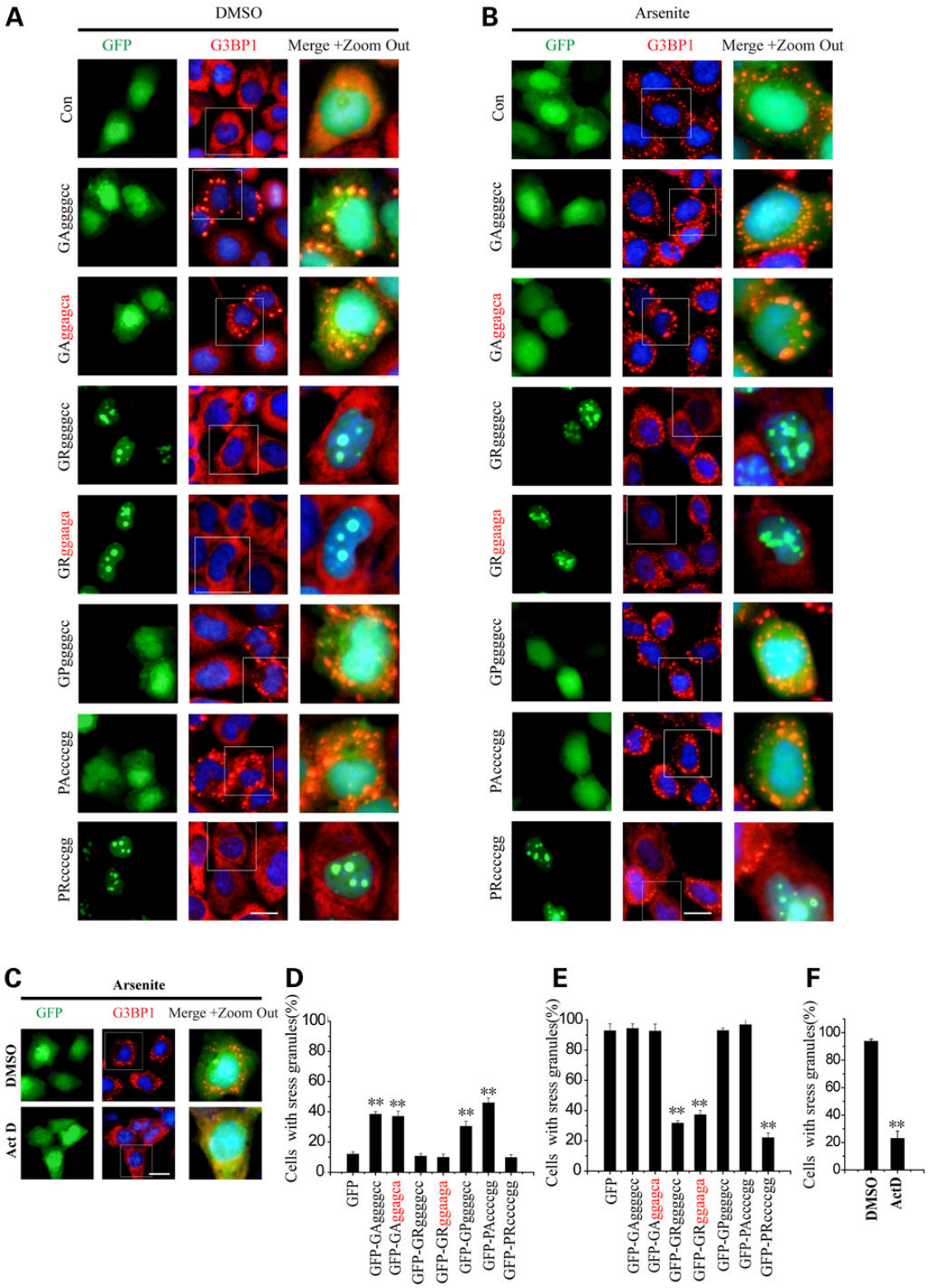

Figure 7. Arginine-containing and non-arginine-containing RAN proteins exerted opposite effects on stress granule formation. (**A**) HEK293 cells were transfected with GFP, GFP-GAggggcc, GFP-GAggagca, GFP-GRggggcc, GFP-GRggaaga, GFP-GPggggcc, GFP-PAccccgg or GFP-PRccccgg. Forty-eight hours later, the cells were subjected to immunofluorescence using an antibody against G3BP1 (red) and stained with DAPI. (**B**) HEK293 cells were transfected as described in A. Forty-eight hours later, the cells were incubated in arsenite (0.5 mM) for 20 min, followed by immunofluorescence using an antibody against G3BP1 (red) and staining with DAPI. (**C**) GFP was transfected into HEK293 cells. Forty-eight hours later, the cells were treated with DMSO or ActD (2 μg/ml) for 4 h, followed by treatment with arsenite (0.5 mM) for 20 min. Subsequently, the cells were fixed, subjected to immunofluorescence using an antibody against G3BP1 (red), and stained with DAPI. (**D–F**) The percentages of transfected cells containing stress granules treated as in A–C were quantified. The results are expressed as the means ± SEM, $^{**}P < 0.01$. The G3BP1 images display the combined G3BP1 and DAPI fluorescent signals. The scale bars represent 10 μm.

aggregate-prone proteins, as previously reported (43). Based on this evidence, the aggregation of most, if not all, pathogenic RAN proteins in patients may represent a downstream effect of the initial toxic effect-induced proteotoxic stress, and RAN protein aggregation may serve as a self-protection process to deposit toxic soluble oligomers, as has been reported for TDP-43 aggregation in ALS/FTD (44) and for polyQ aggregation in Huntington's disease (45).

Interestingly and importantly, the interactome from our mass spectrometry analysis of the synthetic poly-GR-interacting proteins included B23, hnRNPs [such as hnRNP A2/B1, which has been genetically linked to ALS (46)], 40S/60S ribosomal proteins and other proteins previously found in the nucleolus (47,48). Most importantly, these binding partners were previously demonstrated to associate with GGGGCC RNA repeats (12,15,17–20) (Fig. 5E). Moreover, the C9orf72-coding protein associates with hnRNP A1 and hnRNP A2/B1 (7), and Kwon *et al.* showed that poly-GR and poly-PR associate with hnRNP A2 (hnRNP A2/B1) (29), indicating a potential functional overlap between the *C9orf72* RNA gain-of-function and protein gain- and loss-of-function mechanisms. Among the hnRNPs that bound to both poly-GR and GGGGCC repeats, hnRNP H is particularly interesting because 72 GGGGCC repeats predominantly colocalized and interacted with hnRNP H and because the depletion of hnRNP H exerted a similar effect to that of GGGGCC repeat expression on target RNA splicing (15), indicating that the loss of hnRNP H splicing function might be an important event in disease pathogenesis.

Our study revealed a pathological link between two RNP-enriched cellular compartments, the nucleolus and stress granules upon nucleolar stress induced by RAN proteins. Studies have shown that nucleolar stress is involved in many human disorders, such as cancer, Parkinson's disease and Huntington's disease (49–51). Furthermore, it has recently been reported that nucleolar stress, in association with NCL and B23 translocation, is a significant characteristic of *C9orf72* ALS patient cells and GGGGCC repeat-expressing cells (18). Here, we further demonstrated that arginine-rich RAN proteins directly affect the master regulator of nucleolar function, B23, which in turn induced nucleolar stress and impaired stress granule formation (Figs 5–7). Given that stress granules are thought to act as dynamic sorting stations for mRNAs in response to stress stimuli, the overall function of stress granules is cellular quality control via the temporary storage of mRNAs, the repression of translation and the deceleration of cell growth during stress, which may help the cell to maintain survival via protein aggregation (52). If this process is blocked under stressful or pathogenic conditions, the cells might be more sensitive to toxicity. We aimed to elucidate the precise roles of five independent RAN proteins in stress granule formation. Based on our findings, stress granule formation was strikingly inhibited in poly-GR- and poly-PR-transfected cells and in ActD-treated cells. Alternatively, the other RAN proteins, which lacked arginine, exerted the opposite effect (Fig. 7). Similarly, poly-GR and poly-PR expression decreased ribosomal RNA biogenesis, whereas poly-GA expression increased it (Fig. 6A). According to the previous studies, rRNA maturation could be induced by cellular stress such as heat-stress and oxidative stress (53,54) and may serve as a source of nutrients (55). In our study, we found that poly-GA RAN protein could significantly enhance stress granule formation, which could also be enhanced under heat-stress and oxidative stress (56). We reasoned that poly-GA proteins could induce cellular stress, which is associated with stress granule formation. In this scenario, the 18S and 28S rRNA maturation may result from poly-GA-mediated cellular stress. Collectively, these previously unrecognized effects of arginine-containing and non-arginine-containing RAN products on ribosomal maturation and RNA granule formation may have important implications for our understanding of the fundamental mechanism underlying C9ALS/FTD and other neurodegenerative disorders.

In conclusion, our study suggests that the dysfunction of essential nucleolar proteins, such as B23, which is induced by RAN translation of the expanded hexanucleotide repeats in *C9orf72*, lead to upstream toxic nucleolar stress, the downstream dysfunction of RNP homeostasis and, ultimately, neurological damage (Fig. 8). These findings are helpful for both understanding the critical events underlying RAN translation-associated pathogenesis and developing effective treatments for C9ALS/FTD. Strategies to block RAN translation or to alleviate nucleolar stress, which may preserve nucleolar function in dysfunctional cells, could aid the development of novel and likely unexpected therapeutic targets.

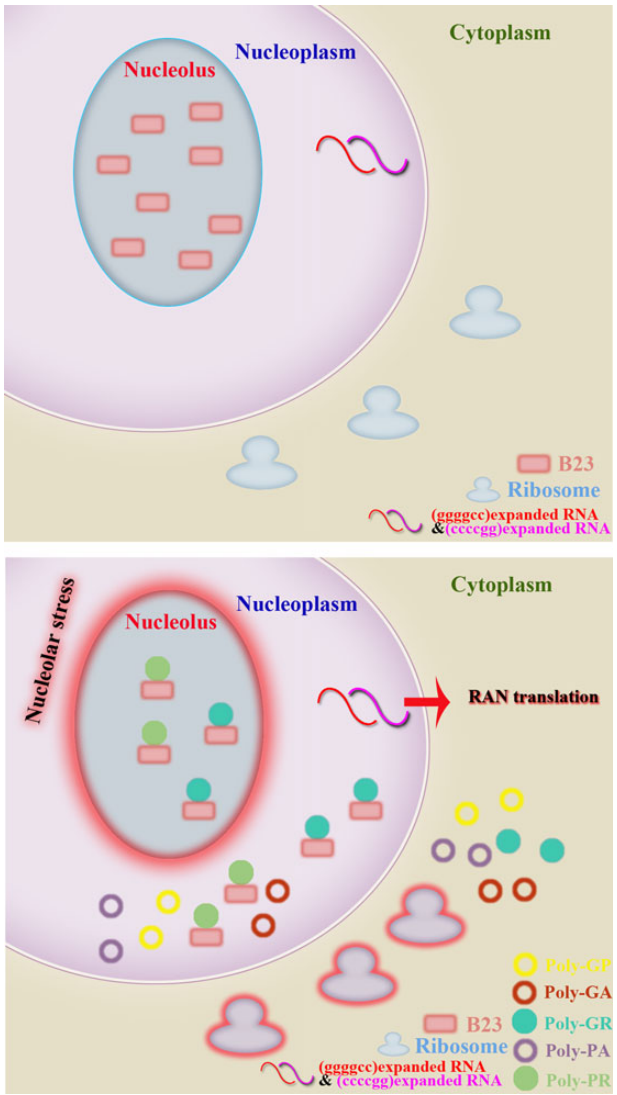

Figure 8. A schematic model illustrating the role of poly-GR and poly-PR in C9orf72 RAN translation-induced cytotoxicity. The results of the present study suggest a simple model in which B23 translocation and nucleolar stress represent the primary molecular determinants of C9ALS/FTD.

Materials and Methods

Plasmid construction

HA-Ub, EGFP-p62, Nhtt-60Q-EGFP, EGFP-N1-ataxin-Q80, EGFP-N1-ataxin-3-Q130, EGFP-N1-ataxin-Q130QF, FLAG-B23 and EGFP-B23 plasmids were described previously (33,57–61).

The 30-repeat No-ATG-ggggcc-GFP sequence was kindly provided by Dr Peng Jin (Emory University, USA). First, using p3 × FLAG-*myc*-CMV-24 (Sigma) as a template, we constructed $FLAG^{-1}$ and $FLAG^{-2}$ plasmids by deleting the nucleotide sequence C or GC preceding the *EcoRI* site via site-directed mutagenesis using the MutanBEST kit (Takara) to produce three distinct reading frames after the *EcoRI* site. The $(ggggcc)_{30}$ repeats were excised from the No-ATG-ggggcc-GFP plasmids and inserted into the C-terminus of p3 × flag-myc-cmv-24, $FLAG^{-1}$ or $FLAG^{-2}$ at EcoRI/BamHI to generate FLAG-GPggggcc, FLAG-GRggggcc and FLAG-GAggggcc, respectively.

To construct plasmids GFP-GPggggcc, GFP-GRggggcc and GFP-GAggggcc, the $(ggggcc)_{30}$ repeats were excised from FLAG-GRggggcc, FLAG-GAggggcc or FLAG-GPggggcc, respectively, and then subcloned into the pEGFP-C1 vector using HindIII and BamHI. To construct plasmids GFP-PAccccgg, the $(ggggcc)_{30}$ repeats obtained from FLAG-GPggggcc via digestion at EcoRI/BamHI were inserted into EGFP-C1 at EcoRI/BglII. To generate the GFP-PRccccgg plasmids, $(ggggcc)_{30}$ repeats obtained from FLAG-GRggggcc via digestion at EcoRI/BamHI were inserted into EGFP-C2 at EcoRI/BglII.

For the synthetic RAN constructs, the $(ggaaga)_{30}$ and $(ggagca)_{30}$ oligonucleotides were synthesized by Invitrogen and subsequently cloned into the pEGFP-N3 vector using EcoRI/SalI sites. We termed these synthetic RAN constructs GRggaaga-GFPN3 and GAggagca-GFPN3, respectively. To generate FLAG-GRggaaga and FLAG-GAggagca, the $(ggaaga)_{30}$ or $(ggagca)_{30}$ repeats were removed from GRggaaga-GFPN3 or GAggagca-GFPN3, respectively, using EcoRI/BamHI and then subcloned into p3 × FLAG-*myc*-CMV-24. GFP-GRggaaga and GFP-GAggagca were generated by subcloning the $(ggaaga)_{30}$ or $(ggagca)_{30}$ repeats from FLAG-GRggaaga or FLAG-GAggagca, respectively, using EcoRI/BamHI and then subcloned into the pEGFP-C1 vector.

To construct plasmids FLAG-GAggagca-long or FLAG-GRggaaga-long, firstly, using pcDNA3.1/myc-HisA (Invitrogen) as template, we constructed $pcDNA3.1^{-2}$ plasmids by deleting nucleotides TG before the EcoRI site using Site Directed Mutagenesis. Secondly, we constructed $pcDNA3.1^{-2}$-$(ggagca)_{30}$ or $pcDNA3.1^{-2}$-$(ggaaga)_{30}$ through cutting $(ggagca)_{30}$ or $(ggaaga)_{30}$ fragments from GAggagca-GFPN3 or GRggaaga-GFPN3 at EcoRI/BamHI sites and inserting them into $pcDNA3.1^{-2}$ plasmids. Then, we subcloned GA$(ggagca)_{30}$ or GR$(ggaaga)_{30}$ from GAggagca-GFPN3 or GRggaaga-GFPN3 through digested at EcoRI/BamHI sites into FLAG at the EcoRI and BglII sites to create $FLAG^{new}$-GAggagca or $FLAG^{new}$-GRggaaga. Finally, FLAG-GAggagca-long or FLAG-GRggaaga-long was generated by subcloning the $(ggagca)_{30}$ or $(ggagca)_{30}$ from $pcDNA3.1^{-2}$-$(ggagca)_{30}$ or $pcDNA3.1^{-2}$-$(ggaaga)_{30}$ into $FLAG^{new}$-GAggagca or $FLAG^{new}$-GRggaaga at EcoRV and BamHI sites.

GFP-GR-TAGggaaga (with STOP) was generated from GFP-GRggaaga via site-directed mutagenesis using the primers 5′ AGCT TCGAATTCCTAGGGAAGAG 3′ and 5′ TGAGCTCGAGATCGTAGT 3′ to generate a TAG stop codon preceding the $(ggaaga)_{30}$ repeats.

All of the constructs were confirmed via sequencing. Detailed sequences and descriptions of the reading frames of our constructs are provided in the Supplementary Material, Figure S7.

Secondary structure prediction of synthetic and pathogenic repeat sequences in RAN constructs

The secondary structure prediction of repeat sequences used in the present study was modeled using MFOLD methodology, which is commonly used to predict the secondary structure of RNA (62). Details are provided in the Supplementary Material.

Cell culture, transfection and chemicals

Human embryonic kidney 293 (HEK293), mouse motor neuron cell line NSC-34, ATG5 WT or KO MEF cells were cultured in Dulbecco's modified Eagle's medium (DMEM) (Gibco) containing 10% fetal bovine serum (FBS) (Gibco) with penicillin (100 U/ml) and streptomycin (100 μg/ml). SH-SY5Y cells were cultured in DMEM/F12 (1 : 1) medium containing 10% FBS with penicillin (100 U/ml) and streptomycin (100 μg/ml). The cells were transfected with Lipofectamine 2000 reagent (Invitrogen) at 30% confluence in DMEM without serum according to the manufacturer's instructions. 4′6-diamidino-2-phenylindole (DAPI), Hoechst 33342, thapsigargin (TG), CHX, actinomycin D (ActD), arsenite and propidium iodide (PI) were purchased from Sigma. MG132 was purchased from Calbiochem, and Bafilomycin A1 (Baf A1) was purchased from Fermentek.

PI staining assay and MTT assay

Cells were incubated PI at room temperature for 15 min and then the positive stained cells (dead cells) were observed using fluorescence microscopy (Olympus IX71). The dead cells were counted, and the quantitative data were shown. For MTT assay, the cells were washed with DMEM without phenol red and incubated with MTT (3-(4,5)-dimethylthiahiazo(-z-y1)-3,5-di-phenytetrazoliumromide, purchased from Sigma) at the concentration of 0.5 mg/ml in DMEM without phenol red. After 3 h, the media were discarded and the formazan crystals were dissolved in DMSO (dimethyl sulfoxide). The optical density was measured by a photometer at 570 nm, and background at 630 nm was subtracted. The quantitative data were normalized to control and the ratios are presented as means ± SE from three independent experiments.

Immunoblot analysis and antibodies

The cells were collected at time indicated after transfection and were lysed in cell lysis buffer [25 mM Tris–HCl (pH 7.6), 1% NP-40, 150 mM NaCl and 1% sodiumdeoxycholate] in the presence of a protease inhibitor cocktail (Roche). Then, the proteins were separated by SDS–PAGE and then transferred onto a polyvinylidene difluoride membrane (Millipore). Immunoblot analysis was performed with the following primary antibodies: monoclonal anti-Nucleophosmin/B23 antibody, polyclonal anti-nucleolin, anti-OPTN, anti-VCP, anti-TDP43 and G3BP1 antibodies were purchased from Proteintech; monoclonal anti-GAPDH antibody was purchased from Millipore, and monoclonal anti-FLAG antibody and monoclonal anti-GFP antibody were purchased from Sigma. Rabbit polyclonal antibody against GFP, anti-HA and anti-LC3 antibodies was described previously (59,60,63).

Immunofluorescence and live cell imaging

For immunofluorescence assay, NSC-34, SH-SY5Y or HEK293 cells were washed with pre-warmed PBS and fixed with 4% paraformaldehyde in PBS at room temperature for 5 min. Cells were

permeabilized with 0.2% Triton X-100 in PBS for 3 min and blocked for 20 min with 0.2% FBS in PBST. Cells were incubated with primary antibody diluted with PBST at room temperature for 3 h, washed lightly with PBST for 5 min. Then, secondary antibody was added and incubated for 1.5 h at room temperature. The following fluorophore-labeled secondary antibodies were used: Alexa Fluor 594 (red)-conjugated Affinipure Donkey Anti-mouse and Anti-rabbit IgG, as well as Alexa Fluor 488 (green)-conjugated Affinipure Donkey Anti-mouse and Anti-rabbit IgG (Invitrogen). Then, the cells were incubated with DAPI (blue), and the live cells were incubated with Hoechst 33342 (blue) for 5 min to visualize the nuclei. Finally, the stained cells or live cells were observed using Zeiss LSM 710 confocal microscopy or fluorescence microscopy (Olympus IX71).

Immunoprecipitation

HEK293 cells transfected with the indicated plasmids were collected 48 h after transfection and lysed in cell lysis buffer. Cell pellet was discarded after centrifugation at 12 000*g* for 20 min at 4°C, and the supernatants were incubated with polyclonal anti-GFP antibody overnight at 4°C. After incubation, protein G Sepharose (Roche) was used for precipitation. The beads were washed three times with W1 buffer [50 mM Tris–HCl (pH 7.6), 1% NP-40, 150 mM NaCl and 1% sodiumdeoxycholate], two times with W2 buffer [25 mM Tris–HCl (pH 7.6), 0.1% NP-40, 500 mM NaCl and 1% sodiumdeoxycholate] and one time with W3 buffer [50 mM Tris–HCl (pH 7.6), 0.1% NP-40 and 1% sodiumdeoxycholate]. Then, the proteins were eluted with SDS sample buffer for immunoblot analysis.

Mass spectrometry analysis

HEK293 cells transfected with GFP or GFP-GRggaaga were lysed, and the cell lysates were immunoprecipitated with anti-GFP antibody and protein G Sepharose (Roche). The proteins were eluted with SDS sample buffer and separated on SDS–PAGE gel, and the gel was subjected to silver staining. Gel lanes were cut into slices, destained, reduced, alkylated and digested with trypsin. Then, the peptides were injected on to an LTQ-Orbitrap Elite (Thermo Fisher Scientific).

Quantitative real-time PCR (qRT-PCR)

Total RNA was extracted from cells using TRIzol Reagent (Invitrogen). Real-time PCR analysis was carried out for quantitative measurement of the target RNA abundance with SYBR Green Real-Time PCR Master Mix (Takara) in a PCR detection system (Applied Biosystems). The following primers were used: 5′ AATCC CATCACCATCTTCCA 3′ and 5′ TGGACTCCACGACGTACTCA 3′ for human GAPDH; 5′ AGAGGTAAACGGGTGGGGTC 3′ and 5′ GGGG TCGGGAGGAACGG 3′ for human 28 s rRNA; 5′ GATGGTAGTC GCCGTGCC 3′ and 5′ GCCTGCTGCCTTCCTTGG 3′ for human 18 s rRNA. The levels of 18 s and 28 s rRNA were normalized to GAPDH.

Supplementary Material

Supplementary Material is available at *HMG* online.

Acknowledgements

We thank Dr Arthur Horwich (Yale University) for critical comments and suggestions on our manuscript; Dr Mingyi Xie, Dr Xinguo Chen (Yale University) and Dr Shengdong Ke (The Rockefeller University) for helpful discussions and suggestions; Dr Peng Jin (Emory University) for providing us the plasmids with GGGGCC repeats; Dr Mian Wu (University of Science and Technology of China) for providing us the FLAG-B23 and EGFP-B23 plasmids; Dr Weidong Le (Baylor College of Medicine, USA) for providing us NSC-34 cells; Dr Chunshan Gui (Soochow University) for providing us HEK293 cells.

Conflict of Interest statement. None declared.

Funding

This work was supported in part by the National High-tech Research and Development program of China 973-projects (2011CB504102), the National Natural Sciences Foundation of China (Nos 31200803 and 31371072), Natural Science Foundation of Jiangsu Province (BK2012181), a Project Funded by Jiangsu Key Laboratory of Translational Research and Therapy for Neuro-Psycho-Diseases (BM2013003) and a Project Funded by the Priority Academic Program Development of Jiangsu Higher Education Institutions.

References

1. DeJesus-Hernandez, M., Mackenzie, I.R., Boeve, B.F., Boxer, A. L., Baker, M., Rutherford, N.J., Nicholson, A.M., Finch, N.A., Flynn, H., Adamson, J. *et al.* (2011) Expanded GGGGCC hexanucleotide repeat in noncoding region of C9ORF72 causes chromosome 9p-linked FTD and ALS. *Neuron*, **72**, 245–256.
2. Renton, A.E., Majounie, E., Waite, A., Simon-Sanchez, J., Rollinson, S., Gibbs, J.R., Schymick, J.C., Laaksovirta, H., van Swieten, J.C., Myllykangas, L. *et al.* (2011) A hexanucleotide repeat expansion in C9ORF72 is the cause of chromosome 9p21-linked ALS-FTD. *Neuron*, **72**, 257–268.
3. Gijselinck, I., Van Langenhove, T., van der Zee, J., Sleegers, K., Philtjens, S., Kleinberger, G., Janssens, J., Bettens, K., Van Cauwenberghe, C., Pereson, S. *et al.* (2012) A C9orf72 promoter repeat expansion in a Flanders-Belgian cohort with disorders of the frontotemporal lobar degeneration-amyotrophic lateral sclerosis spectrum: a gene identification study. *Lancet Neurol.*, **11**, 54–65.
4. Majounie, E., Abramzon, Y., Renton, A.E., Perry, R., Bassett, S. S., Pletnikova, O., Troncoso, J.C., Hardy, J., Singleton, A.B. and Traynor, B.J. (2012) Repeat expansion in C9ORF72 in Alzheimer's disease. *N. Engl. J. Med.*, **366**, 283–284.
5. Hensman Moss, D.J., Poulter, M., Beck, J., Hehir, J., Polke, J.M., Campbell, T., Adamson, G., Mudanohwo, E., McColgan, P., Haworth, A. *et al.* (2014) C9orf72 expansions are the most common genetic cause of Huntington disease phenocopies. *Neurology*, **82**, 292–299.
6. Gomez-Tortosa, E., Gallego, J., Guerrero-Lopez, R., Marcos, A., Gil-Neciga, E., Sainz, M.J., Diaz, A., Franco-Macias, E., Trujillo-Tiebas, M.J., Ayuso, C. *et al.* (2013) C9ORF72 hexanucleotide expansions of 20-22 repeats are associated with frontotemporal deterioration. *Neurology*, **80**, 366–370.
7. Farg, M.A., Sundaramoorthy, V., Sultana, J.M., Yang, S., Atkinson, R.A., Levina, V., Halloran, M.A., Gleeson, P.A., Blair, I.P., Soo, K.Y. *et al.* (2014) C9ORF72, implicated in amytrophic lateral sclerosis and frontotemporal dementia, regulates endosomal trafficking. *Hum. Mol. Genet.*, **23**, 3579–3595.
8. Ciura, S., Lattante, S., Le Ber, I., Latouche, M., Tostivint, H., Brice, A. and Kabashi, E. (2013) Loss of function of C9orf72 causes motor deficits in a zebrafish model of amyotrophic lateral sclerosis. *Ann. Neurol.*, **74**, 180–187.

9. Therrien, M., Rouleau, G.A., Dion, P.A. and Parker, J.A. (2013) Deletion of C9ORF72 results in motor neuron degeneration and stress sensitivity in *C. elegans*. *PLoS One*, **8**, e83450.
10. Sicot, G. and Gomes-Pereira, M. (2013) RNA toxicity in human disease and animal models: from the uncovering of a new mechanism to the development of promising therapies. *Biochim. Biophys. Acta.*, **1832**, 1390–1409.
11. Mizielinska, S., Lashley, T., Norona, F.E., Clayton, E.L., Ridler, C.E., Fratta, P. and Isaacs, A.M. (2013) C9orf72 frontotemporal lobar degeneration is characterised by frequent neuronal sense and antisense RNA foci. *Acta Neuropathol.*, **126**, 845–857.
12. Donnelly, C.J., Zhang, P.W., Pham, J.T., Heusler, A.R., Mistry, N. A., Vidensky, S., Daley, E.L., Poth, E.M., Hoover, B., Fines, D.M. *et al.* (2013) RNA toxicity from the ALS/FTD C9ORF72 expansion is mitigated by antisense intervention. *Neuron*, **80**, 415–428.
13. Gendron, T.F., Bieniek, K.F., Zhang, Y.J., Jansen-West, K., Ash, P.E., Caulfield, T., Daughrity, L., Dunmore, J.H., Castanedes-Casey, M., Chew, J. *et al.* (2013) Antisense transcripts of the expanded C9ORF72 hexanucleotide repeat form nuclear RNA foci and undergo repeat-associated non-ATG translation in c9FTD/ALS. *Acta Neuropathol.*, **126**, 829–844.
14. Lagier-Tourenne, C., Baughn, M., Rigo, F., Sun, S., Liu, P., Li, H. R., Jiang, J., Watt, A.T., Chun, S., Katz, M. *et al.* (2013) Targeted degradation of sense and antisense C9orf72 RNA foci as therapy for ALS and frontotemporal degeneration. *Proc. Natl Acad. Sci. USA*, **110**, E4530–e84539.
15. Lee, Y.B., Chen, H.J., Peres, J.N., Gomez-Deza, J., Attig, J., Stalekar, M., Troakes, C., Nishimura, A.L., Scotter, E.L., Vance, C. *et al.* (2013) Hexanucleotide repeats in ALS/FTD form length-dependent RNA foci, sequester RNA binding proteins, and are neurotoxic. *Cell Rep.*, **5**, 1178–1186.
16. Zu, T., Liu, Y., Banez-Coronel, M., Reid, T., Pletnikova, O., Lewis, J., Miller, T.M., Harms, M.B., Falchook, A.E., Subramony, S.H. *et al.* (2013) RAN proteins and RNA foci from antisense transcripts in C9ORF72 ALS and frontotemporal dementia. *Proc. Natl Acad. Sci. USA*, **110**, E4968–E4977.
17. Xu, Z., Poidevin, M., Li, X., Li, Y., Shu, L., Nelson, D.L., Li, H., Hales, C.M., Gearing, M., Wingo, T.S. *et al.* (2013) Expanded GGGGCC repeat RNA associated with amyotrophic lateral sclerosis and frontotemporal dementia causes neurodegeneration. *Proc. Natl Acad. Sci. USA*, **110**, 7778–7783.
18. Haeusler, A.R., Donnelly, C.J., Periz, G., Simko, E.A., Shaw, P.G., Kim, M.S., Maragakis, N.J., Troncoso, J.C., Pandey, A., Sattler, R. *et al.* (2014) C9orf72 nucleotide repeat structures initiate molecular cascades of disease. *Nature*, **507**, 195–200.
19. Almeida, S., Gascon, E., Tran, H., Chou, H.J., Gendron, T.F., Degroot, S., Tapper, A.R., Sellier, C., Charlet-Berguerand, N., Karydas, A. *et al.* (2013) Modeling key pathological features of frontotemporal dementia with C9ORF72 repeat expansion in iPSC-derived human neurons. *Acta Neuropathol.*, **126**, 385–399.
20. Mori, K., Lammich, S., Mackenzie, I.R., Forne, I., Zilow, S., Kretzschmar, H., Edbauer, D., Janssens, J., Kleinberger, G., Cruts, M. *et al.* (2013) hnRNP A3 binds to GGGGCC repeats and is a constituent of p62-positive/TDP43-negative inclusions in the hippocampus of patients with C9orf72 mutations. *Acta Neuropathol.*, **125**, 413–423.
21. Zu, T., Gibbens, B., Doty, N.S., Gomes-Pereira, M., Huguet, A., Stone, M.D., Margolis, J., Peterson, M., Markowski, T.W., Ingram, M.A. *et al.* (2011) Non-ATG-initiated translation directed by microsatellite expansions. *Proc. Natl Acad. Sci. USA*, **108**, 260–265.
22. Ash, P.E., Bieniek, K.F., Gendron, T.F., Caulfield, T., Lin, W.L., Dejesus-Hernandez, M., van Blitterswijk, M.M., Jansen-West, K., Paul, J.W. 3rd, Rademakers, R. *et al.* (2013) Unconventional translation of C9ORF72 GGGGCC expansion generates insoluble polypeptides specific to c9FTD/ALS. *Neuron*, **77**, 639–646.
23. Mori, K., Weng, S.M., Arzberger, T., May, S., Rentzsch, K., Kremmer, E., Schmid, B., Kretzschmar, H.A., Cruts, M., Van Broeckhoven, C. *et al.* (2013) The C9orf72 GGGGCC repeat is translated into aggregating dipeptide-repeat proteins in FTLD/ALS. *Science*, **339**, 1335–1338.
24. Todd, P.K., Oh, S.Y., Krans, A., He, F., Sellier, C., Frazer, M., Renoux, A.J., Chen, K.C., Scaglione, K.M., Basrur, V. *et al.* (2013) CGG repeat-associated translation mediates neurodegeneration in fragile X tremor ataxia syndrome. *Neuron*, **78**, 440–455.
25. Mori, K., Arzberger, T., Grasser, F.A., Gijselinck, I., May, S., Rentzsch, K., Weng, S.M., Schludi, M.H., van der Zee, J., Cruts, M. *et al.* (2013) Bidirectional transcripts of the expanded C9orf72 hexanucleotide repeat are translated into aggregating dipeptide repeat proteins. *Acta Neuropathol.*, **126**, 881–893.
26. Mann, D.M., Rollinson, S., Robinson, A., Bennion Callister, J., Thompson, J.C., Snowden, J.S., Gendron, T., Petrucelli, L., Masuda-Suzukake, M., Hasegawa, M. *et al.* (2013) Dipeptide repeat proteins are present in the p62 positive inclusions in patients with frontotemporal lobar degeneration and motor neurone disease associated with expansions in C9ORF72. *Acta Neuropathol. Commun.*, **1**, 68.
27. Taylor, J.P. (2013) Neuroscience. RNA that gets RAN in neurodegeneration. *Science*, **339**, 1282–1283.
28. Mizielinska, S., Gronke, S., Niccoli, T., Ridler, C.E., Clayton, E. L., Devoy, A., Moens, T., Norona, F.E., Woollacott, I.O., Pietrzyk, J. *et al.* (2014) C9orf72 repeat expansions cause neurodegeneration in Drosophila through arginine-rich proteins. *Science*, **345**, 1192–1194.
29. Kwon, I., Xiang, S., Kato, M., Wu, L., Theodoropoulos, P., Wang, T., Kim, J., Yun, J., Xie, Y. and McKnight, S.L. (2014) Poly-dipeptides encoded by the C9orf72 repeats bind nucleoli, impede RNA biogenesis, and kill cells. *Science*, **345**, 1139–1145.
30. Ross, C.A. and Poirier, M.A. (2005) Opinion: what is the role of protein aggregation in neurodegeneration? *Nat. Rev. Mol. Cell Biol.*, **6**, 891–898.
31. Ying, Z., Wang, H. and Wang, G. (2013) The ubiquitin proteasome system as a potential target for the treatment of neurodegenerative diseases. *Curr. Pharm. Des.*, **19**, 3305–3314.
32. Rubinsztein, D.C. (2006) The roles of intracellular protein-degradation pathways in neurodegeneration. *Nature*, **443**, 780–786.
33. Yao, Z., Duan, S., Hou, D., Wang, W., Wang, G., Liu, Y., Wen, L. and Wu, M. (2010) B23 acts as a nucleolar stress sensor and promotes cell survival through its dynamic interaction with hnRNPU and hnRNPA1. *Oncogene*, **29**, 1821–1834.
34. Avitabile, D., Bailey, B., Cottage, C.T., Sundararaman, B., Joyo, A., McGregor, M., Gude, N., Truffa, S., Zarrabi, A., Konstandin, M. *et al.* (2011) Nucleolar stress is an early response to myocardial damage involving nucleolar proteins nucleostemin and nucleophosmin. *Proc. Natl Acad. Sci. USA*, **108**, 6145–6150.
35. Lindstrom, M.S. and Zhang, Y. (2008) Ribosomal protein S9 is a novel B23/NPM-binding protein required for normal cell proliferation. *J. Biol. Chem.*, **283**, 15568–15576.
36. Suzuki, A., Kogo, R., Kawahara, K., Sasaki, M., Nishio, M., Maehama, T., Sasaki, T., Mimori, K. and Mori, M. (2012) A new PICTure of nucleolar stress. *Cancer Sci.*, **103**, 632–637.
37. Li, Y.R., King, O.D., Shorter, J. and Gitler, A.D. (2013) Stress granules as crucibles of ALS pathogenesis. *J. Cell Biol.*, **201**, 361–372.

38. Ramaswami, M., Taylor, J.P. and Parker, R. (2013) Altered ribostasis: RNA-protein granules in degenerative disorders. *Cell*, **154**, 727–736.
39. Gendron, T.F., Belzil, V.V., Zhang, Y.J. and Petrucelli, L. (2014) Mechanisms of toxicity in C9FTLD/ALS. *Acta Neuropathol.*, **127**, 359–376.
40. Fratta, P., Poulter, M., Lashley, T., Rohrer, J.D., Polke, J.M., Beck, J., Ryan, N., Hensman, D., Mizielinska, S., Waite, A.J. *et al.* (2013) Homozygosity for the C9orf72 GGGGCC repeat expansion in frontotemporal dementia. *Acta Neuropathol.*, **126**, 401–409.
41. Sareen, D., O'Rourke, J.G., Meera, P., Muhammad, A.K., Grant, S., Simpkinson, M., Bell, S., Carmona, S., Ornelas, L., Sahabian, A. *et al.* (2013) Targeting RNA foci in iPSC-derived motor neurons from ALS patients with a C9ORF72 repeat expansion. *Sci. Transl. Med.*, **5**, 208ra149.
42. Mackenzie, I.R., Arzberger, T., Kremmer, E., Troost, D., Lorenzl, S., Mori, K., Weng, S.M., Haass, C., Kretzschmar, H.A., Edbauer, D. *et al.* (2013) Dipeptide repeat protein pathology in C9ORF72 mutation cases: clinico-pathological correlations. *Acta Neuropathol.*, **126**, 859–879.
43. Oma, Y., Kino, Y., Sasagawa, N. and Ishiura, S. (2004) Intracellular localization of homopolymeric amino acid-containing proteins expressed in mammalian cells. *J. Biol. Chem.*, **279**, 21217–21222.
44. Cragnaz, L., Klima, R., Skoko, N., Budini, M., Feiguin, F. and Baralle, F.E. (2014) Aggregate formation prevents dTDP-43 neurotoxicity in the Drosophila melanogaster eye. *Neurobiol. Dis.*, **71**, 74–80.
45. Arrasate, M., Mitra, S., Schweitzer, E.S., Segal, M.R. and Finkbeiner, S. (2004) Inclusion body formation reduces levels of mutant huntingtin and the risk of neuronal death. *Nature*, **431**, 805–810.
46. Kim, H.J., Kim, N.C., Wang, Y.D., Scarborough, E.A., Moore, J., Diaz, Z., MacLea, K.S., Freibaum, B., Li, S., Molliex, A. *et al.* (2013) Mutations in prion-like domains in hnRNPA2B1 and hnRNPA1 cause multisystem proteinopathy and ALS. *Nature*, **495**, 467–473.
47. Andersen, J.S., Lyon, C.E., Fox, A.H., Leung, A.K., Lam, Y.W., Steen, H., Mann, M. and Lamond, A.I. (2002) Directed proteomic analysis of the human nucleolus. *Curr. Biol.*, **12**, 1–11.
48. Scherl, A., Coute, Y., Deon, C., Calle, A., Kindbeiter, K., Sanchez, J.C., Greco, A., Hochstrasser, D. and Diaz, J.J. (2002) Functional proteomic analysis of human nucleolus. *Mol. Biol. Cell*, **13**, 4100–4109.
49. Parlato, R. and Liss, B. (2014) How Parkinson's disease meets nucleolar stress. *Biochim. Biophys. Acta*, **1842**, 791–797.
50. Lee, J., Hwang, Y.J., Ryu, H. and Kowall, N.W. (2014) Nucleolar dysfunction in Huntington's disease. *Biochim. Biophys. Acta*, **1842**, 785–790.
51. Boulon, S., Westman, B.J., Hutten, S., Boisvert, F.M. and Lamond, A.I. (2010) The nucleolus under stress. *Mol. Cell*, **40**, 216–227.
52. Anderson, P. and Kedersha, N. (2009) RNA granules: post-transcriptional and epigenetic modulators of gene expression. *Nat. Rev. Mol. Cell Biol.*, **10**, 430–436.
53. Chen, X., Wurtmann, E.J., Van Batavia, J., Zybailov, B., Washburn, M.P. and Wolin, S.L. (2007) An ortholog of the Ro autoantigen functions in 23S rRNA maturation in *D. radiodurans*. *Genes Develop*, **21**, 1328–1339.
54. Chen, X., Taylor, D.W., Fowler, C.C., Galan, J.E., Wang, H.W. and Wolin, S.L. (2013) An RNA degradation machine sculpted by Ro autoantigen and noncoding RNA. *Cell*, **153**, 166–177.
55. Deutscher, M.P. (2006) Degradation of RNA in bacteria: comparison of mRNA and stable RNA. *Nucl. Acids Res.*, **34**, 659–666.
56. Kedersha, N. and Anderson, P. (2007) Mammalian stress granules and processing bodies. *Methods Enzymol.*, **431**, 61–81.
57. Ying, Z., Wang, H., Fan, H., Zhu, X., Zhou, J., Fei, E. and Wang, G. (2009) Gp78, an ER associated E3, promotes SOD1 and ataxin-3 degradation. *Hum. Mol. Genet.*, **18**, 4268–4281.
58. Wang, H., Jia, N., Fei, E., Wang, Z., Liu, C., Zhang, T., Fan, J., Wu, M., Chen, L., Nukina, N. *et al.* (2007) p45, an ATPase subunit of the 19S proteasome, targets the polyglutamine disease protein ataxin-3 to the proteasome. *J. Neurochem.*, **101**, 1651–1661.
59. Wang, H., Ying, Z. and Wang, G. (2012) Ataxin-3 regulates aggresome formation of copper-zinc superoxide dismutase (SOD1) by editing K63-linked polyubiquitin chains. *J. Biol. Chem.*, **287**, 28576–28585.
60. Zhou, L., Wang, H.F., Ren, H.G., Chen, D., Gao, F., Hu, Q.S., Fu, C., Xu, R.J., Ying, Z. and Wang, G.H. (2013) Bcl-2-dependent upregulation of autophagy by sequestosome 1/p62 in vitro. *Acta Pharmacol. Sin.*, **34**, 651–656.
61. Zhou, L., Wang, H., Chen, D., Gao, F., Ying, Z. and Wang, G. (2014) p62/Sequestosome 1 regulates aggresome formation of pathogenic Ataxin-3 with expanded polyglutamine. *Int. J. Mol. Sci.*, **15**, 14997–15010.
62. Zuker, M. (2003) Mfold web server for nucleic acid folding and hybridization prediction. *Nucl. Acids Res.*, **31**, 3406–3415.
63. Ying, Z., Wang, H., Fan, H. and Wang, G. (2011) The endoplasmic reticulum (ER)-associated degradation system regulates aggregation and degradation of mutant neuroserpin. *J. Biol. Chem.*, **286**, 20835–20844.